

## RESEARCH LETTER

10.1002/2017GL076077

## Key Points:

- Surface biological responses precede SST responses during the ENSO cycle
- Iron is the key factor that enables the surface chlorophyll to rapidly reflect the subsurface ocean response to ENSO
- Incorporating the biological precursor into the SST-based ENSO prediction model suggests potential to improve seasonal prediction skill

## Supporting Information:

- Supporting Information S1

## Correspondence to:

J.-Y. Park,  
jongyeon@princeton.edu

## Citation:

Park, J.-Y., Dunne, J. P., & Stock, C. A. (2018). Ocean chlorophyll as a precursor of ENSO: An Earth system modeling study. *Geophysical Research Letters*, 45, 1939–1947. <https://doi.org/10.1002/2017GL076077>

Received 18 OCT 2017

Accepted 8 FEB 2018

Accepted article online 12 FEB 2018

Published online 26 FEB 2018

## Ocean Chlorophyll as a Precursor of ENSO: An Earth System Modeling Study

Jong-Yeon Park<sup>1,2</sup> , John P. Dunne<sup>2</sup> , and Charles A. Stock<sup>2</sup> 

<sup>1</sup>Atmospheric and Oceanic Sciences Program, Princeton University, Princeton, NJ, USA, <sup>2</sup>Geophysical Fluid Dynamics Laboratory, National Oceanic and Atmospheric Administration, Princeton, NJ, USA

**Abstract** Ocean chlorophyll concentration, a proxy for phytoplankton, is strongly influenced by internal ocean dynamics such as those associated with El Niño–Southern Oscillation (ENSO). Observations show that ocean chlorophyll responses to ENSO generally lead sea surface temperature (SST) responses in the equatorial Pacific. A long-term global Earth system model simulation incorporating marine biogeochemical processes also exhibits a preceding chlorophyll response. In contrast to simulated SST anomalies, which significantly lag the wind-driven subsurface heat response to ENSO, chlorophyll anomalies respond rapidly. Iron was found to be the key factor connecting the simulated surface chlorophyll anomalies to the subsurface ocean response. Westerly wind bursts decrease central Pacific chlorophyll by reducing iron supply through wind-driven thermocline deepening but increase western Pacific chlorophyll by enhancing the influx of coastal iron from the maritime continent. Our results mechanistically support the potential for chlorophyll-based indices to inform seasonal ENSO forecasts beyond previously identified SST-based indices.

## 1. Introduction

Variability of phytoplankton in the tropical Pacific is mostly controlled by variations in nutrients supplied to the well-lit euphotic zone (Pennington et al., 2006). This variability is dominated by the El Niño–Southern Oscillation (ENSO), which is the largest source of interannual climate variability in the tropical Pacific (McPhaden et al., 2006). Satellite-derived ocean color data, that is, chlorophyll concentration (proxy for phytoplankton), have motivated extensive studies of the basin-scale biological and physical coupling during ENSO events. Initial analysis of the satellite data reported the lowest level of tropical chlorophyll on record during the 1997–1998 El Niño period followed by a dramatic recovery in mid-1998 (Behrenfeld et al., 2001; Chavez et al., 1999; Murtugudde et al., 1999; Radenac et al., 2001). With the accumulation of the data, statistical approaches for analyzing the biological disturbances during ENSO cycle have been attempted (Park et al., 2011; Radenac et al., 2012; Turk et al., 2011; Yoder & Kennelly, 2003). Dominant mechanisms governing the chlorophyll response to ENSO include changes in equatorial upwelling and thermocline depth (Chavez et al., 1999; Radenac et al., 2001; Wilson & Coles, 2005), and zonal advection (Picaut et al., 2001; Radenac et al., 2012; Stoens et al., 1999), all linked to atmosphere–ocean coupling. Specifically, during El Niño years, westerly wind anomalies over the equatorial Pacific result in overall oligotrophic conditions by suppression of equatorial upwelling of nutrient-rich deep waters and eastward advection of nutrient-poor/warm-pool waters. This leads to an overall inverse relationship between the chlorophyll and sea surface temperature (SST) anomalies in the tropical Pacific.

Although previous studies using satellite data broadened our understanding of the phytoplankton–ENSO relationship, most works cited above focused on the response of ocean chlorophyll concurrent with and following the ENSO SST response (Behrenfeld et al., 2001; Park et al., 2011; Radenac et al., 2001). This approach restricts analysis of the ocean chlorophyll response to a passive indicator of SST response. However, observational and modeling evidence suggests that the chlorophyll response along the equator often leads the SST response in the ENSO cycle (e.g., Figures 7c and 7f in Park et al., 2011, and Figures 6a and 6b in Lee et al., 2014). This leading response, particularly during the onset phase of ENSO, and its implications have been overlooked in the previous studies. It implies that the overall inverse relationship between the surface chlorophyll and SST during the ENSO mature season does not always hold during different phases of ENSO. Furthermore, understanding such bio-physical coupling process in different phases of ENSO can provide additional insight into the temporal evolution of the biological response to ENSO and may have important implications for the predictability of marine biogeochemistry.

Here we investigate the basin-wide characteristics of chlorophyll variability in different phases of the ENSO cycle and its underlying mechanisms. A long-term global Earth system model simulation is shown to exhibit a preceding chlorophyll response to ENSO transitions evident in the temporally limited satellite record. Insights gained from the model simulation shed light on the mechanism driving the evolution of biological and physical variables during the ENSO cycle. We combine this mechanistic understanding with the lead-lag relationship between the chlorophyll and SST responses to explore the value of chlorophyll indices for ENSO prediction relative to surface and depth-integrated physical predictors.

## 2. Data and Methods

Model output for this study is drawn from a long preindustrial control simulation of Geophysical Fluid Dynamics Laboratory Earth System Model (GFDL-ESM2M) (Dunne et al., 2012, 2013). The model consists of an atmospheric model (AM2), a land model (LM2.1), a Modular Ocean Model Version 4 (MOM4p1), and a Sea Ice Simulator (SIS). This is integrated with a marine ecosystem model, the Carbon, Ocean Biogeochemistry and Lower Trophics (COBALT) (Stock et al., 2014a, 2014b). COBALT considers 33 tracers to resolve global-scale cycles of dissolved organic/inorganic species with three phytoplankton and three zooplankton groups. The horizontal resolution of the atmosphere and land models is  $2.5^\circ$  longitude  $\times$   $2^\circ$  latitude on a regular grid, while ocean and sea ice model have the resolution of  $1^\circ$  with telescoping to  $1/3^\circ$  meridional spacing near the equator.

Different versions of ESM2M have been used in a variety of studies including climate change experiments, global carbon cycle, bio-climate interactions, and predictability of marine biogeochemistry (Krasting et al., 2014; Park et al., 2013; Stock et al., 2017). Simulated marine biogeochemistry by GFDL's Earth system models has been shown to capture the observed large-scale mean pattern as well as the ENSO-driven temporal variation of marine biogeochemistry (Laufkotter et al., 2015; Park et al., 2014; Stock et al., 2014b). Moreover, the physical component of the ESM2M produces realistic ENSO simulation, being ranked highly among Coupled Model Intercomparison Project (CMIP)-class climate models (Guilyardi, 2006; Kug et al., 2010; van Oldenborgh et al., 2005; Wittenberg et al., 2006). In this study, the model is integrated for 1,500 years with a constant, preindustrial carbon dioxide ( $\text{CO}_2$ ), and the last 500 years from the integration are analyzed.

The observational chlorophyll and SST data analyzed here are monthly mean fields obtained from the GlobColour products (<http://www.globcolour.info>) and from the National Oceanic and Atmospheric Administration optimum interpolation SST product (<https://www.esrl.noaa.gov>), respectively (Maritorena & Siegel, 2005; Reynolds et al., 2002). The GlobColour product is the merged ocean color data from different satellite sensors, which ensures the bias reduction along with increased coverage and consistency. For both SST and chlorophyll data, anomalies are defined relative to the climatological monthly mean during the period SEP1997-FEB2017 for which chlorophyll data are available. The monthly chlorophyll and SST data are provided on a  $1.0^\circ$  grid, and the results shown here are consistent regardless of the spatial resolution of data we used. In this study, ENSO events are defined according to  $\pm 1$  standard deviation exceedance of the wintertime (November–January) NINO3.4 ( $170^\circ$ – $120^\circ$ W,  $5^\circ$ S– $5^\circ$ N) SST index. Given that the evolution of each ENSO event is slightly different, the onset, mature, and decaying phases of El Niño are uniquely defined for the observation and model according to the occurrence timing of positive, maximum, and negative NINO3.4 SST anomalies, respectively, within a broad seasonal period.

The primary method used to analyze the observation and model data is linear regression analysis. The statistical ENSO prediction model used to test the performance of springtime (February to April) chlorophyll-based indices in predicting ENSO events is equivalent to the conventional multilinear regression method that estimates the predictand (i.e., NINO3.4 SST index in our study) from multiple explanatory variables. Thus, while the results shown in this study are presented as El Niño progression, the analogous but opposite progression occurs during La Niña events.

## 3. Results

### 3.1. Chlorophyll and SST Responses to ENSO

As mentioned in the introduction, tropical chlorophyll and SST anomalies in El Niño years have an overall inverse relationship due to reduced equatorial upwelling that increases SST but decreases nutrient supply from deeper water. The observed chlorophyll and SST anomalies regressed onto the ENSO index

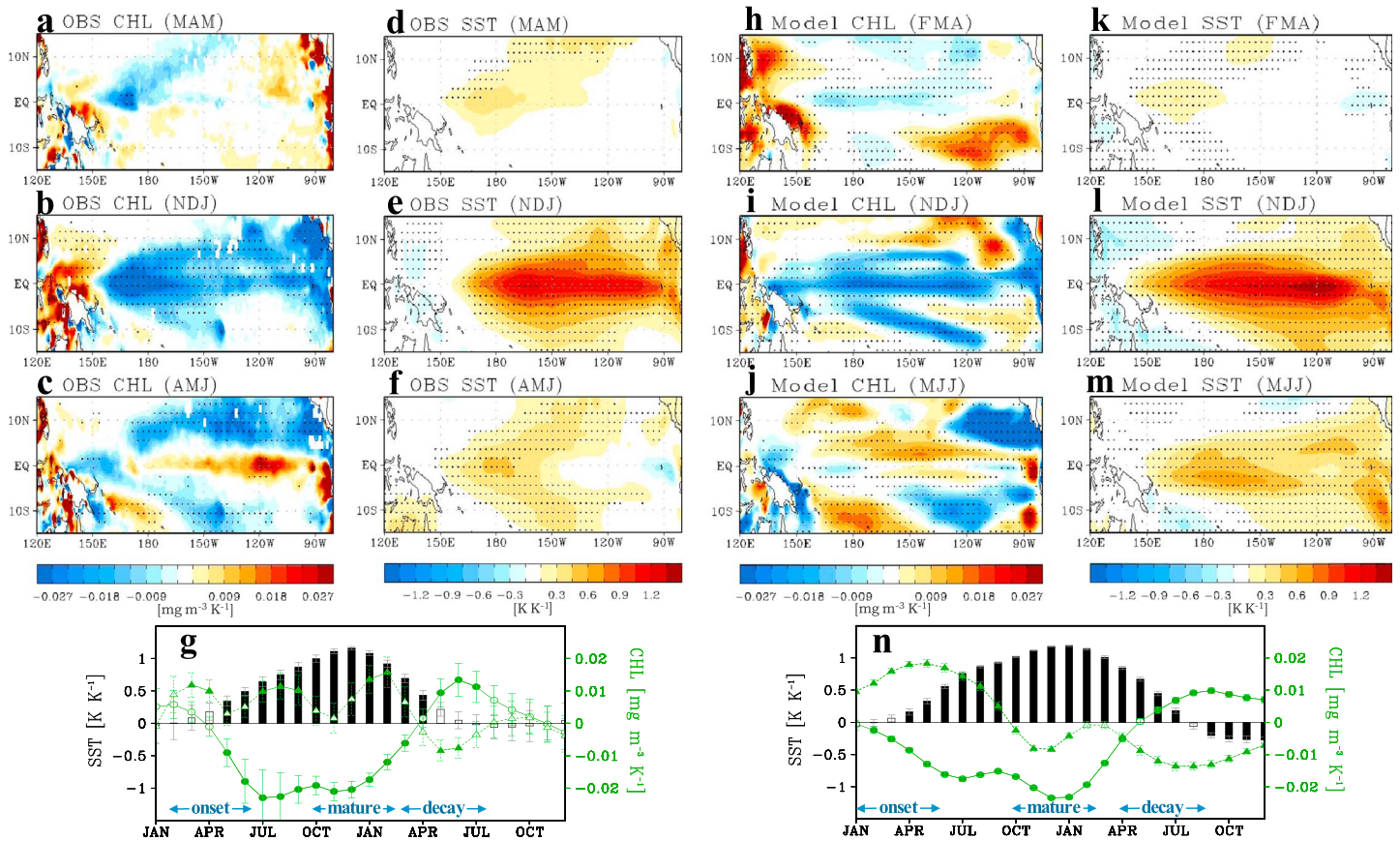


**Figure 1.** Observed (a–c) chlorophyll and (d–f) sea surface temperature (SST) anomalies during the onset, mature, and decaying phases of El Niño. The simulated patterns are the regressed anomalies against the boreal winter (November–January) ENSO index (NINO3.4: 170°W–120°W, 5°S–5°N). The stippled regions denote the 95% confidence region according to two-tailed *t* test. (g) The evolution of regressed chlorophyll (green line with circles) and SST (black bar) anomalies averaged in the equatorial central Pacific (180°–120°W, 2°S–2°N). The chlorophyll anomaly averaged in the western Pacific (140°–160°E, 5°S–0°N) is shown as green line with triangles. The anomalies are smoothed using a three-month running mean, and the filled marks/bars represent significant values at 95% confidence level. The error bars represent the standard error interval of regressed anomalies. (h–n) Similar to (a–g) but use modeled data rather than observationally based fields. Note that the green triangles in n use slightly different region for the western Pacific chlorophyll anomaly (140°–160°E, 10°S–0°N).

(i.e., NINO3.4 SST anomalies) illustrate well this inverse relationship. Negative chlorophyll anomalies prevail in the equatorial Pacific during the mature phase of El Niño, and significant positive chlorophyll anomalies prevail in the far western Pacific where negative SST anomalies occur (Figures 1b and 1e). This inverse relationship, however, does not hold across all El Niño phases. For example, significant positive chlorophyll anomalies have already started to develop in the equatorial central Pacific (CP) during the decaying phase of El Niño, while positive SST anomalies still prevail in the tropical Pacific (Figures 1c, 1f, and 1g). A similar feature can be observed in the onset phase of El Niño, showing the significant positive chlorophyll anomalies in the western Pacific before the presence of significant equatorial SST signals (Figure 1g). These rapid changes in seasonal chlorophyll anomalies result in substantial changes in the timing of the summer phytoplankton bloom. During the onset phase of the 2009–2010 El Niño, for example, the equatorial phytoplankton bloom (chlorophyll concentration > 0.2 mg/m<sup>3</sup>) starts in July, a delay of about 2 months compared to the climatological mean bloom (starting in May). In the decaying phase, the bloom starts in the middle of March, 1.5 months earlier than the climatological bloom (Figure S1). Other El Niño events over the recent decades for which the satellite chlorophyll data are available show similar behaviors of chlorophyll response preceding the SST response during the onset and decaying phases of El Niño (Figure S2). While the satellite sample size is limited, events that have been observed suggest that chlorophyll responses during the ENSO cycle may have a lead relationship with SST responses in the equatorial Pacific.

The potential lead relationship between chlorophyll and SST responses is examined further in the 500-year-long simulation by the Earth system model (Figures 1h–1n). Consistent with the observation shown in

**Table 1**  
*Percentage of ENSO Events That the Chlorophyll Response Precedes the SST Response During the Onset and Decaying Phases of ENSO Simulated From the 500-Year-Long Control Experiment*

	Onset phase		Decaying phase	
	El Niño	La Niña	El Niño	La Niña
Leading cases	79% (33)	86% (42)	93% (57)	92% (23)
Simultaneous cases	12% (5)	10% (5)	3% (2)	8% (2)
Lagging cases	9% (4)	4% (2)	3% (2)	0% (0)

*Note.* El Niño–Southern Oscillation (ENSO) years are defined when the wintertime (November–January) NINO3.4 SST index exceeds its own  $\pm 1$  standard deviation ( $\sigma$ ). Leading and lagging cases are defined based on the timing when anomalies of chlorophyll and SST exceed  $\pm 0.2\sigma$  during ENSO onset and decay phases; thus, the El Niño (La Niña) events in which positive (negative) SST anomalies exceeding  $\pm 0.2\sigma$  persist for more than two consecutive winters are excluded. Leading and lagging cases are those when the chlorophyll response precedes or follows the SST response by at least one month, and otherwise considered as simultaneous cases. Numbers in parentheses represent the number of each case.

Figures 1a–1g, the simulated chlorophyll and SST during the onset and decaying phases of El Niño also show the chlorophyll response preceding the SST response. In the onset phase of El Niño, significant negative chlorophyll anomalies already occur in the central equatorial Pacific. Meanwhile, the El Niño signal exhibits only weak positive SST anomalies confined in the western Pacific (Figures 1h, 1k, and 1n). In the El Niño decaying phase, the strong negative chlorophyll anomalies developed during the El Niño mature phase already turn into positive anomalies, while the SST anomaly remains in positive (Figures 1j, 1m, and 1n). The evolution of monthly chlorophyll and SST anomaly averaged in the equatorial CP further indicates a 1.5 month delay of the SST anomaly sign reversal during the El Niño onset phase and a 3 month delay during the El Niño decaying phase compared to the sign reversal of equatorial chlorophyll anomalies (Figure 1n).

To further assess the robustness of the preceding chlorophyll response, we examined how often the chlorophyll response precedes the SST response during the ENSO cycle. The chlorophyll preceding cases constitute 75% of

El Niño onset cases and 93% of El Niño decaying cases (Table 1). This is in dramatic contrast to 9% and 3% of chlorophyll lagging cases during El Niño onset and decaying phases, respectively. Similar statistics can be found for La Niña events: 86% and 92% preceding cases during La Niña onset and decaying phases, respectively. We also analyze the same statistics by separating El Niño events into two groups, those followed by La Niña events (97% of chlorophyll leading cases) and those not (89% of chlorophyll leading cases), which shows consistent results with those shown in Table 1 for each of these subgroups. Overall, modeling results join the limited observational evidence in supporting a generally robust lead relationship between chlorophyll and SST across ENSO cycle transition.

### 3.2. Mechanisms Underlying the Preceding Chlorophyll Response

With the foregoing evidence that the chlorophyll response precedes the SST response during the onset and decaying phases of ENSO, the vertical structure of simulated biological and physical responses to ENSO is examined to elucidate its detailed mechanism. Here we focus on the springtime bio-physical responses in the onset phase of El Niño.

The chlorophyll anomalies shown in Figure 1h are consistent throughout the mixed layer of about 20–50 m (Figure 2a). The negative chlorophyll anomaly centered around the date-line extends across the equatorial Pacific, and the positive anomaly appears in the far western Pacific. An inverse relationship is found between the upper and lower level chlorophyll anomalies. This is attributed to the self-shading effect by the presence of phytoplankton in the water column (Manizza et al., 2005; Morel, 1988). The reduced chlorophyll concentration in the upper ocean during the El Niño event allows more light penetration at depth, leading to a deeper subsurface chlorophyll maximum.

In contrast to the chlorophyll anomalies mostly confined in the top 100 m, the temperature response in the El Niño onset phase shows the strongest signal in the subsurface layer of 100–200 m depth (Figure 2b). This subsurface positive temperature anomaly reflects the deepening of the thermocline associated with westerly wind-forced downwelling Kelvin wave that propagates eastward, forming a major component of the thermocline depth change in the central and eastern Pacific (EP) (Kessler & McPhaden, 1995). Because the deepened thermocline has to first reduce the zonal SST gradient and then alters the winds and equatorial upwelling, which takes a couple of months, the SST anomaly in the EP generally shows a delayed response to the wind-driven subsurface temperature response.

Surface chlorophyll anomalies, however, more rapidly reflect the subsurface response during the onset phase of El Niño. The responses of two major nutrients, nitrate and iron, show the strongest negative anomalies in the subsurface ocean (Figures 2d and 2e), which is consistent with the subsurface temperature response (Figure 2b). This is because the nutricline, where the vertical gradient of phytoplankton nutrients has a maximum, mostly coincides with the thermocline (Barber & Chavez, 1991). However, the two nutrients show opposite responses near the surface. Iron exhibits a negative anomaly that is associated with decreased

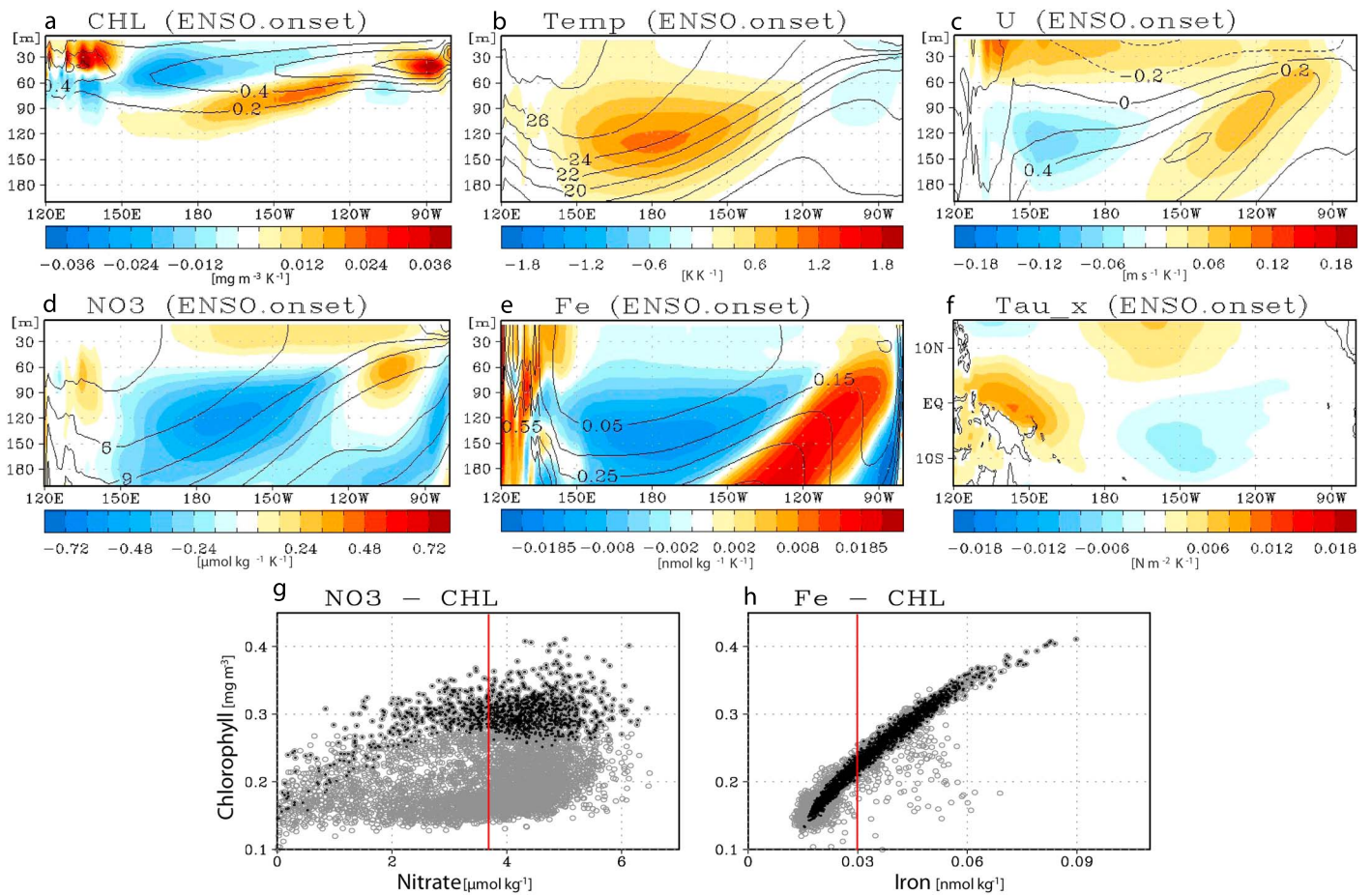


**Figure 2.** Equatorial cross sections of springtime (a) chlorophyll, (b) temperature, (c) zonal current, (d) nitrate, and (e) iron anomalies during the ENSO onset phase (February–April). (f) The spatial map of zonal wind stress anomaly during the same period. Contours represent the climatological mean and shadings represent the regressed anomalies against the boreal winter (November–January) NINO3.4 index. Iron limitation in the equatorial Pacific is represented by scatter plots: Monthly mean (g) nitrate versus chlorophyll and (h) iron versus chlorophyll in the equatorial Pacific (150°E–150°W, 2°S–2°N). The black dots overlapped with gray dots represent the cases when the iron concentration is greater than 0.04 nmol/kg for (g), and the nitrate concentration is greater than 4 μmol/kg for (h). The vertical red lines in (g) and (h) indicate the climatological mean values of nitrate and iron in the equatorial Pacific.

surface chlorophyll and increased surface nitrate. This response is consistent with the observed iron limitation in the equatorial Pacific (Behrenfeld et al., 2006; Coale et al., 1996): less iron leads to less phytoplankton that consume less nitrate. Comparison of nutrient/chlorophyll relationships across the equatorial Pacific further confirms the dominance of iron as a chlorophyll control (Figures 2g–2h): Surface chlorophyll increases consistently with increasing iron but has a far weaker relationship with nitrate. This iron-limited relationship is even more obvious in the conditional case when each of the nutrients is sufficiently high (black dots overlapped with gray dots in Figures 2g–2h), showing that the mean of equatorial Pacific nitrate (vertical red line in Figures 2g–2h) is already in the range of the saturated regime so that the nitrate impact may be nonsignificant, which is not the case for iron. Other nutrients, such as phosphate and silicate, also exhibit similar behaviors as in the nitrate case (Figure S3).

The decreased iron concentration in the overall equatorial Pacific during El Niño is due to the reduced upward iron flux associated with the deepening of the nutricline. The short time-scales of this local vertical reorganization of the water column, combined with the high sensitivity of surface chlorophyll to iron enrichment at low iron concentrations (Figure 2h), lead to a rapid chlorophyll response. This contrasts with the time delay of the temperature response involving the oceanic wave propagation, wind changes, and accumulated heat in the mixed layer. In the far western Pacific, the increased iron is related to the eastward advection of iron-rich water from the New Guinea shelf (Ryan et al., 2006), which is confined in the western Pacific due to the climatological westward current in the central equatorial Pacific (Figure 2c).

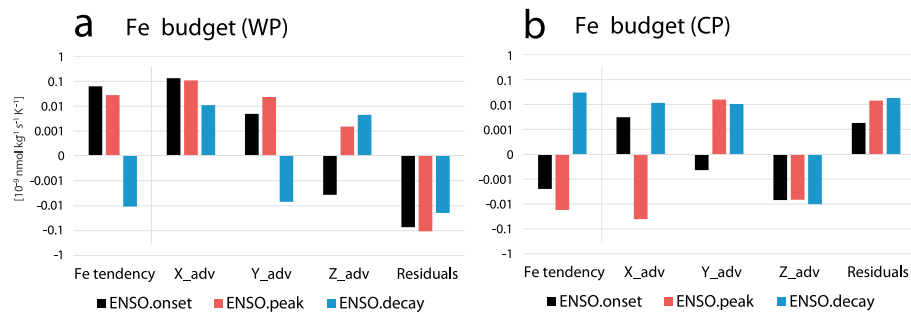


**Figure 3.** Iron budget terms averaged over the upper 50 m depth in the (a) western (140°–160°E; 2°S–2°N) and (b) central equatorial Pacific (160°E–150°W; 2°S–2°N). Iron tendency term ( $\frac{\partial Fe}{\partial t}$ ) is decomposed into four terms: Zonal advection ( $-u \frac{\partial Fe}{\partial x}$ ), meridional advection ( $-v \frac{\partial Fe}{\partial y}$ ), vertical advection ( $-w \frac{\partial Fe}{\partial z}$ ), and residuals (e.g., biological processes and small-scale oceanic diffusion). Each term is the regressed anomaly against the boreal winter (November–January) NINO3.4 index and is shown during the onset (black), mature (red), and decaying (blue) phases of ENSO. The ordinate is shown on a logarithmic scale.

An iron budget analysis further confirms that the chlorophyll decrease in the central equatorial Pacific is dominated by the vertical advection of iron during the onset phase of El Niño (Figure 3b). Given that the Equatorial Undercurrent shapes the subsurface iron concentration as seen in Figure 2, the reduced vertical advection of equatorial iron during the El Niño onset supports the deepening of the thermocline and Equatorial Undercurrent that prevents iron supply to the euphotic layer. This vertical advection-dominating process during the El Niño onset contrasts with the horizontal advection-dominating process during the mature and decaying phases of El Niño. In the far western Pacific, the chlorophyll increase is more dominated by the horizontal advection of iron than the vertical process across different El Niño phases (Figure 3a).

### 3.3. Predictability of ENSO Using Equatorial Chlorophyll

As the surface chlorophyll rapidly reflects the atmosphere-driven subsurface ocean response, we now assess the potential of springtime chlorophyll anomalies as a predictor of ENSO. Given that the statistical ENSO prediction models based on historical SST have shown lower predictive skill than dynamical prediction models during the spring months preceding ENSO events (Barnston et al., 2012), the springtime surface chlorophyll reflecting the atmosphere forcing and subsurface ocean response could potentially improve seasonal forecasts of ENSO.

We construct a statistical ENSO prediction model and compare the performance of springtime (February to April) chlorophyll-based indices with that of previously used SST indices in predicting ENSO in the following winter (November to January). Two springtime chlorophyll indices and three springtime SST indices are used to predict the wintertime NINO3.4 ENSO index in this model. Two springtime chlorophyll indices are averaged in the western Pacific and the equatorial Pacific, respectively, where significant chlorophyll anomalies are present in Figure 1h. Three SST indices are the western Pacific SST index averaged in the area where significant SST anomalies appear in Figure 1k, the North Pacific Gyre Oscillation index defined by the second principal components of north Pacific SST anomalies (Di Lorenzo et al., 2008), and the north tropical Atlantic SST index averaged in the tropical Atlantic region between 0° and 15°N. The North Pacific Gyre Oscillation and north tropical Atlantic SST anomalies are known springtime precursors of ENSO, which are capable of exciting an equatorial ENSO signal in the following summer and fall (Ham et al., 2013; Vimont et al., 2003). The statistical model shows that using the two springtime chlorophyll indices gives a better performance in predicting ENSO in the following winter (corr. = 0.63) than using the three SST-based indices (corr. = 0.53). The prediction skill here is defined by the correlation of the predicted wintertime NINO3.4 SST index from the multiregression model with the simulated NINO3.4 index from GFDL-ESM2M. Combining SST-based prediction with chlorophyll indices further improves the seasonal prediction skill to 0.68.

A regression model based on an ensemble learning approach is applied to assess the importance of these biological and physical predictors. For this analysis, we expand our predictor set to include warm water volume and sea surface height. Unlike SST, but like chlorophyll, these physical variables represent the subsurface ENSO signals and have been shown to improve predictive skill (Clarke & Van Gorder, 2003; Xue et al., 2000). The importance of each predictor is estimated by the errors that would be introduced to the prediction if a particular predictor is permuted (Friedman, 2001). The result shows that the two chlorophyll-based

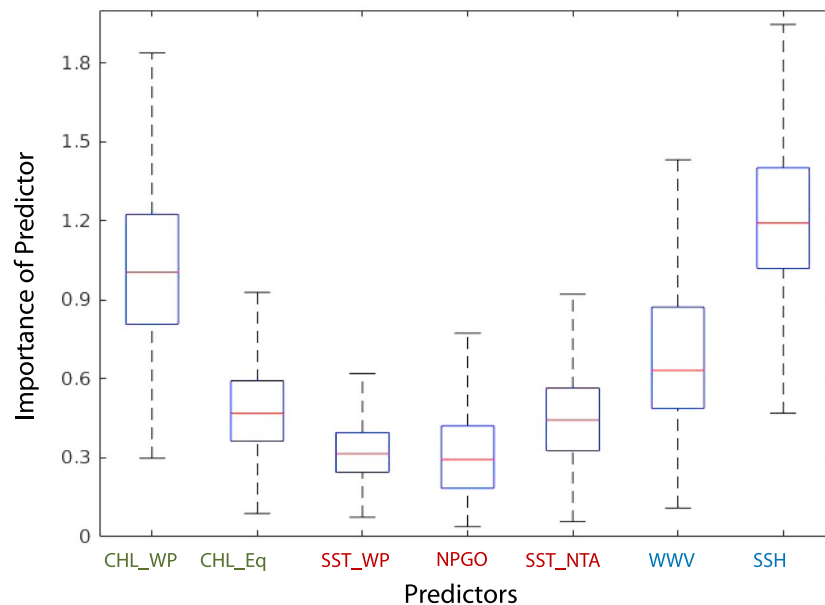


**Figure 4.** The box-and-whisker plot of the importance of springtime (February–April) predictors for the following wintertime (November–January) ENSO according to a regression model that takes an ensemble learning approach for prediction. The predictors are grouped into three categories: chlorophyll-based indices (green), sea surface temperature (SST)-based indices (red), and subsurface condition indices (blue). Those indices are western Pacific chlorophyll (140°–160°E, 10°S–0°N), central equatorial chlorophyll (160°E–150°W, 2°S–2°N), western Pacific SST (150°E–150°W, 5°S–5°N), North Pacific Gyre Oscillation (second principal component of north Pacific SST), north tropical Atlantic SST (90°W–20°E, 0°S–15°N), warm water volume (WWV) in the tropical Pacific (over 20 °C in 120°E–110°W, 5°S–5°N, 0–500 m), and equatorial sea surface height (140°E–120°W, 5°S–5°N). The importance of predictor shown is normalized by scaling each value with the median of the predictor importance value of western Pacific chlorophyll index.

indices are generally ranked higher than the SST-based indices (Figure 4). The importance of chlorophyll is similar to that of warm water volume and sea surface height, supporting that the underlying mechanisms of chlorophyll and subsurface heat anomalies are based on the same physical process. In particular, the importance of western Pacific chlorophyll index as a springtime predictor turns out to be significantly higher than those of all three SST-based indices.

#### 4. Conclusions

The surface chlorophyll response to ENSO generally precedes the SST response during the ENSO cycle across satellite-observed ENSO events. This prominent aspect of equatorial chlorophyll dynamics has received limited attention in previous studies. This study shows that the preceding chlorophyll response is robustly reproduced in Earth system model simulations. While the SST response is a delayed signal of the thermocline change fully manifesting only after zonal Kelvin wave propagation, surface chlorophyll rapidly reflects the subsurface signal due to the rapid biological response to iron flux changes.

Recent studies have emphasized the diversity of ENSO events (Capotondi et al., 2015). The Earth system model, ESM2M, used in this study produces both EP and CP El Niño events similar to observations, including the modest independence of CP and EP SST anomalies during El Niño events (Figures S4 and S5). Given the good performance of the model in simulating different types of El Niño, we separate the statistics shown in Table 1 into two groups, that is, EP El Niño and CP El Niño types. We find that regardless of El Niño types, the percentage of chlorophyll leading cases is much higher than that of lagging or simultaneous cases (Table S1). This robust leading chlorophyll response across ENSO types is presumably related to common mechanisms during the charge/discharge cycle of ENSO involving atmospheric disturbances, excitation of equatorial waves, and thermocline changes.

We acknowledge the limitation of this single model-based study of biophysical coupling processes. A multimodel-based approach would be useful for further evaluating the preceding chlorophyll response. However, examining the ENSO-driven biological response using Earth system models is often challenging due to large differences in model skill (Laufkotter et al., 2015). For example, many Earth system models still

suffer from uncertainties in both physical and biological variables and they often fail to simulate the observed ENSO-driven chlorophyll variation (Figures S6 and S7). While biases remain in our model, it does successfully capture the large-scale biogeochemical response to ENSO in quantitative and qualitative ways (Figure S7g). This includes the iron-limited ocean ecosystem in the equatorial Pacific and the preceding chlorophyll response in the onset and decaying phases of ENSO.

Marine biogeochemical variables in the tropics are generally controlled by physical processes in the ocean; thus, they are often treated as passive tracers just following the change in physical variables. This study, however, furthers evidence that surface chlorophyll responds to ENSO evolution earlier than the surface temperature and elucidates mechanisms capable of producing this response. This mechanistic understanding may provide theoretical support for the potential inclusion of springtime chlorophyll-based indices in statistical ENSO prediction models. Our initial tests incorporating this biological precursor into the SST-based ENSO prediction models suggest potential to improve seasonal prediction skill. The equatorial surface chlorophyll response integrates the subsurface ocean response to wind forcing and could eventually serve as an alternative ENSO predictor to physical variables that convey subsurface oceanic heat content information. However, the desire to incorporate chlorophyll as an alternative predictor should be strongly tempered by the limited direct observational evidence afforded by the abbreviated satellite record. Further exploration of underlying mechanisms, extension of the satellite time series, and probationary exploration in an ensemble context is advisable. Significant advances are required to bridge the understanding and empirical gap between physical and chlorophyll based metrics for predictive use.

#### Acknowledgments

The authors would like to thank the anonymous reviewers for helpful and constructive comments on the manuscript. We would also like to thank Robbie Toggweiler and Fernando Gonzalez-Taboada for internal reviews of the manuscript. This study was supported by NOAA's marine ecosystem tipping point initiative. The model simulation data used here are archived at GFDL (<ftp://nomads.gfdl.noaa.gov/users/Jong-Yeon.Park/CHL-ENSO/GFDL-ESM2M-COBALT/>). The updated simulation data will soon be available in the CMIP6 archive. The CMIP5 data used for supporting information are downloaded from the Earth System Grid Federation (ESGF) archive (<https://esgf-node.llnl.gov/projects/esgf-llnl/>) made available by the World Climate Research Programme Working Group on Coupled Modeling and by climate modeling groups.

#### References

- Barber, R. T., & Chavez, F. P. (1991). Regulation of primary productivity rate in the equatorial Pacific. *Limnology and Oceanography*, *36*(8), 1803–1815.
- Barnston, A. G., Tippett, M. K., L'Heureux, M. L., Li, S. H., & DeWitt, D. G. (2012). Skill of real-time seasonal ENSO model predictions during 2002–11: Is our capability increasing? *Bulletin of the American Meteorological Society*, *93*(5), 631–651. <https://doi.org/10.1175/BAMS-D-11-00111.1>
- Behrenfeld, M. J., Randerson, J. T., McClain, C., Feldman, G. C., Los, S. O., Tucker, C. J., et al. (2001). Biospheric primary production during an ENSO transition. *Science*, *291*(5513), 2594–2597. <https://doi.org/10.1126/science.1055071>
- Behrenfeld, M. J., Worthington, K., Sherrell, R. M., Chavez, F. P., Strutton, P., McPhaden, M., & Shea, D. M. (2006). Controls on tropical Pacific Ocean productivity revealed through nutrient stress diagnostics. *Nature*, *442*(7106), 1025–1028. <https://doi.org/10.1038/nature05083>
- Capotondi, A., Wittenberg, A. T., Newman, M., di Lorenzo, E., Yu, J. Y., Braconnot, P., et al. (2015). Understanding ENSO diversity. *Bulletin of the American Meteorological Society*, *96*(6), 921–938. <https://doi.org/10.1175/BAMS-D-13-00117.1>
- Chavez, F. P., Strutton, P. G., Friederich, C. E., Feely, R. A., Feldman, G. C., Foley, D. C., & McPhaden, M. J. (1999). Biological and chemical response of the equatorial Pacific Ocean to the 1997–98 El Niño. *Science*, *286*(5447), 2126–2131. <https://doi.org/10.1126/science.286.5447.2126>
- Clarke, A. J., & Van Gorder, S. (2003). Improving El Niño prediction using a space-time integration of Indo-Pacific winds and equatorial Pacific upper ocean heat content. *Geophysical Research Letters*, *30*(7), 1399. <https://doi.org/10.1029/2002GL016673>
- Coale, K. H., Johnson, K. S., Fitzwater, S. E., Gordon, R. M., Tanner, S., Chavez, F. P., et al. (1996). A massive phytoplankton bloom induced by an ecosystem-scale iron fertilization experiment in the equatorial Pacific Ocean. *Nature*, *383*(6600), 495–501. <https://doi.org/10.1038/383495a0>
- Di Lorenzo, E., Schneider, N., Cobb, K. M., Franks, P. J. S., Chhak, K., Miller, A. J., et al. (2008). North Pacific gyre oscillation links ocean climate and ecosystem change. *Geophysical Research Letters*, *35*, L08607. <https://doi.org/10.1029/2007GL032838>
- Dunne, J. P., John, J. G., Adcroft, A. J., Griffies, S. M., Hallberg, R. W., Shevliakova, E., et al. (2012). GFDL's ESM2 global coupled climate-carbon Earth system models. Part I: Physical formulation and baseline simulation characteristics. *Journal of Climate*, *25*(19), 6646–6665. <https://doi.org/10.1175/JCLI-D-11-00560.1>
- Dunne, J. P., John, J. G., Shevliakova, E., Stouffer, R. J., Krasting, J. P., Malyshev, S. L., et al. (2013). GFDL's ESM2 global coupled climate-carbon Earth system models. Part II: Carbon system formulation and baseline simulation characteristics. *Journal of Climate*, *26*(7), 2247–2267. <https://doi.org/10.1175/JCLI-D-12-00150.1>
- Friedman, J. H. (2001). Greedy function approximation: A gradient boosting machine. *Annals of Statistics*, *29*(5), 1189–1232. <https://doi.org/10.1214/aos/1013203451>
- Guilyardi, E. (2006). El Niño-mean state-seasonal cycle interactions in a multi-model ensemble. *Climate Dynamics*, *26*(4), 329–348. <https://doi.org/10.1007/s00382-005-0084-6>
- Ham, Y.-G., Kug, J.-S., Park, J.-Y., & Jin, F.-F. (2013). Sea surface temperature in the north tropical Atlantic as a trigger for El Niño/Southern Oscillation events. *Nature Geoscience*, *6*(2), 112–116. <https://doi.org/10.1038/ngeo1686>
- Kessler, W. S., & McPhaden, M. J. (1995). Oceanic equatorial waves and the 1991–93 El Niño. *Journal of Climate*, *8*(7), 1757–1774. [https://doi.org/10.1175/1520-0442\(1995\)008%3C1757:OEWATE%3E2.0.CO;2](https://doi.org/10.1175/1520-0442(1995)008%3C1757:OEWATE%3E2.0.CO;2)
- Krasting, J. P., Dunne, J. P., Shevliakova, E., & Stouffer, R. J. (2014). Trajectory sensitivity of the transient climate response to cumulative carbon emissions. *Geophysical Research Letters*, *41*, 2520–2527. <https://doi.org/10.1002/2013GL059141>
- Kug, J. S., Choi, J., An, S. I., Jin, F. F., & Wittenberg, A. T. (2010). Warm pool and cold tongue El Niño events as simulated by the GFDL 2.1 coupled GCM. *Journal of Climate*, *23*(5), 1226–1239.
- Laufkötter, C., Vogt, M., Gruber, N., Aita-Noguchi, M., Aumont, O., Bopp, L., et al. (2015). Drivers and uncertainties of future global marine primary production in marine ecosystem models. *Biogeosciences*, *12*(23), 6955–6984. <https://doi.org/10.5194/bg-12-6955-2015>
- Lee, K. W., Yeh, S. W., Kug, J. S., & Park, J. Y. (2014). Ocean chlorophyll response to two types of El Niño events in an ocean-biogeochemical coupled model. *Journal of Geophysical Research: Oceans*, *119*, 933–952. <https://doi.org/10.1002/2013JC009050>
- Manizza, M., Le Quéré, C., Watson, A. J., & Buitenhuis, E. T. (2005). Bio-optical feedbacks among phytoplankton, upper ocean physics and sea-ice in a global model. *Geophysical Research Letters*, *32*, L05603. <https://doi.org/10.1029/2004GL020778>

- Maritorena, S., & Siegel, D. A. (2005). Consistent merging of satellite ocean color data sets using a bio-optical model. *Remote Sensing of Environment*, 94(4), 429–440. <https://doi.org/10.1016/j.rse.2004.08.014>
- McPhaden, M. J., Zebiak, S. E., & Glantz, M. H. (2006). ENSO as an integrating concept in Earth science. *Science*, 314(5806), 1740–1745. <https://doi.org/10.1126/science.1132588>
- Morel, A. (1988). Optical modeling of the Upper Ocean in relation to its Biogenous matter content (case I waters). *Journal of Geophysical Research*, 93(C9), 10749–10,768. <https://doi.org/10.1029/JC093iC09p10749>
- Murtugudde, R. G., Signorini, S. R., Christian, J. R., Busalacchi, A. J., McClain, C. R., & Picaut, J. (1999). Ocean color variability of the tropical indo-Pacific basin observed by SeaWiFS during 1997–1998. *Journal of Geophysical Research*, 104(C8), 18,351–18,366. <https://doi.org/10.1029/1999JC900135>
- Park, J. Y., Kug, J. S., Park, J., Yeh, S. W., & Jang, C. J. (2011). Variability of chlorophyll associated with El Niño-Southern Oscillation and its possible biological feedback in the equatorial Pacific. *Journal of Geophysical Research*, 116, C10001. <https://doi.org/10.1029/2011JC007056>
- Park, J. Y., Kug, J. S., & Park, Y. G. (2014). An exploratory modeling study on bio-physical processes associated with ENSO. *Progress in Oceanography*, 124, 28–41. <https://doi.org/10.1016/j.pocean.2014.03.013>
- Park, J. Y., Kug, J. S., Seo, H., & Bader, J. (2013). Impact of bio-physical feedbacks on the tropical climate in coupled and uncoupled GCMs. *Climate Dynamics*, 1–17.
- Pennington, J. T., Mahoney, K. L., Kuwahara, V. S., Kolber, D. D., Calienes, R., & Chavez, F. P. (2006). Primary production in the eastern tropical Pacific: A review. *Progress in Oceanography*, 69(2–4), 285–317. <https://doi.org/10.1016/j.pocean.2006.03.012>
- Picaut, J., Ioualalen, M., Delcroix, T., Masia, F., Murtugudde, R., & Vialard, J. (2001). The oceanic zone of convergence on the eastern edge of the Pacific warm pool: A synthesis of results and implications for El Niño-Southern Oscillation and biogeochemical phenomena. *Journal of Geophysical Research*, 106(C2), 2363–2386. <https://doi.org/10.1029/2000JC900141>
- Radenac, M. H., Leger, F., Singh, A., & Delcroix, T. (2012). Sea surface chlorophyll signature in the tropical Pacific during eastern and central Pacific ENSO events. *Journal of Geophysical Research*, 117, C04007. <https://doi.org/10.1029/2011JC007841>
- Radenac, M. H., Menkes, C., Vialard, J., Moulin, C., Dandonneau, Y., Delcroix, T., et al. (2001). Modeled and observed impacts of the 1997–1998 El Niño on nitrate and new production in the equatorial Pacific. *Journal of Geophysical Research*, 106(C11), 26,879–26,898. <https://doi.org/10.1029/2000JC000546>
- Reynolds, R. W., Rayner, N. A., Smith, T. M., Stokes, D. C., & Wang, W. Q. (2002). An improved in situ and satellite SST analysis for climate. *Journal of Climate*, 15(13), 1609–1625. [https://doi.org/10.1175/1520-0442\(2002\)015%3C1609:AISAS%3E2.0.CO;2](https://doi.org/10.1175/1520-0442(2002)015%3C1609:AISAS%3E2.0.CO;2)
- Ryan, J. P., Ueki, I., Chao, Y., Zhang, H. C., Polito, P. S., & Chavez, F. P. (2006). Western Pacific modulation of large phytoplankton blooms in the central and eastern equatorial Pacific. *Journal of Geophysical Research*, 111, G02013. <https://doi.org/10.1029/2005JG000084>
- Stock, C. A., Dunne, J. P., & John, J. G. (2014a). Drivers of trophic amplification of ocean productivity trends in a changing climate. *Biogeosciences*, 11(24), 7125–7135. <https://doi.org/10.5194/bg-11-7125-2014>
- Stock, C. A., Dunne, J. P., & John, J. G. (2014b). Global-scale carbon and energy flows through the marine planktonic food web: An analysis with a coupled physical-biological model. *Progress in Oceanography*, 120, 1–28. <https://doi.org/10.1016/j.pocean.2013.07.001>
- Stock, C. A., John, J. G., Rykaczewski, R. R., Asch, R. G., Cheung, W. W. L., Dunne, J. P., et al. (2017). Reconciling fisheries catch and ocean productivity. *Proceedings of the National Academy of Sciences of the United States of America*, 114(8), E1441–E1449. <https://doi.org/10.1073/pnas.1610238114>
- Stoens, A., Menkès, C., Radenac, M. H., Dandonneau, Y., Grima, N., Eldin, G., et al. (1999). The coupled physical-new production system in the equatorial Pacific during the 1992–1995 El Niño. *Journal of Geophysical Research*, 104(C2), 3323–3339. <https://doi.org/10.1029/98JC02713>
- Turk, D., Meinen, C. S., Antoine, D., McPhaden, M. J., & Lewis, M. R. (2011). Implications of changing El Niño patterns for biological dynamics in the equatorial Pacific Ocean. *Geophysical Research Letters*, 38, L23603. <https://doi.org/10.1029/2011GL049674>
- van Oldenborgh, G. J., Philip, S. Y., & Collins, M. (2005). El Niño in a changing climate: a multi-model study. *Ocean Science*, 1(2), 81–95. <https://doi.org/10.5194/os-1-81-2005>
- Vimont, D. J., Wallace, J. M., & Battisti, D. S. (2003). The seasonal footprinting mechanism in the Pacific: Implications for ENSO. *Journal of Climate*, 16(16), 2668–2675. [https://doi.org/10.1175/1520-0442\(2003\)016%3C2668:TSMFIT%3E2.0.CO;2](https://doi.org/10.1175/1520-0442(2003)016%3C2668:TSMFIT%3E2.0.CO;2)
- Wilson, C., & Coles, V. J. (2005). Global climatological relationships between satellite biological and physical observations and upper ocean properties. *Journal of Geophysical Research*, 110, C10001. <https://doi.org/10.1029/2004JC002724>
- Wittenberg, A. T., Rosati, A., Lau, N. C., & Ploshay, J. J. (2006). GFDL's CM2 global coupled climate models. Part III: Tropical Pacific climate and ENSO. *Journal of Climate*, 19(5), 698–722. <https://doi.org/10.1175/JCLI3631.1>
- Xue, Y., Leetmaa, A., & Ji, M. (2000). ENSO prediction with Markov models: The impact of sea level. *Journal of Climate*, 13(4), 849–871. [https://doi.org/10.1175/1520-0442\(2000\)013%3C0849:EPWMMT%3E2.0.CO;2](https://doi.org/10.1175/1520-0442(2000)013%3C0849:EPWMMT%3E2.0.CO;2)
- Yoder, J. A., & Kennelly, M. A. (2003). Seasonal and ENSO variability in global ocean phytoplankton chlorophyll derived from 4 years of SeaWiFS measurements. *Global Biogeochemical Cycles*, 17(4), 1112. <https://doi.org/10.1029/2002GB001942>